https://doi.org/10.1093/plphys/kiab575 PLANT PHYSIOLOGY 2022: 188: 1649–1664

Plant Physiology®

Research Article

Boron uptake in rice is regulated post-translationally via a clathrin-independent pathway

Sheng Huang [1], Noriyuki Konishi,[1] Naoki Yamaji [1], Ji Feng Shao,[1,2] Namiki Mitani-Ueno [1] and Jian Feng Ma [1,*,†]

1 Institute of Plant Science and Resources, Okayama University, Kurashiki 710-0046, Japan
2 State Key Laboratory of Subtropical Silviculture, Zhejiang A&F University, Zhejiang 311300, China

*Author for communication: maj@rib.okayama-u.ac.jp
These authors contributed equally (S.H., N.K., N.Y.).
†Senior author

S.H., N.K., N.Y., and J.F.M. conceived and designed the experiments. S.H., N.K., N.Y., J.F.S., N.M.U., and J.F.M. performed the experiments and analyzed data. S.H. and J.F.M. wrote the paper. All authors discussed the results and commented on the manuscript.
The author responsible for distribution of materials integral to the findings presented in this article in accordance with the policy described in the Instructions for Authors (https://academic.oup.com/plphys/pages/general-instructions) is Jian Feng Ma (maj@rib.okayama-u.ac.jp).

Abstract

Uptake of boron (B) in rice (*Oryza sativa*) is mediated by the Low silicon rice 1 (OsLsi1) channel, belonging to the NOD26-like intrinsic protein III subgroup, and the efflux transporter B transporter 1 (OsBOR1). However, it is unknown how these transporters cooperate for B uptake and how they are regulated in response to B fluctuations. Here, we examined the response of these two transporters to environmental B changes at the transcriptional and posttranslational level. OsBOR1 showed polar localization at the proximal side of both the exodermis and endodermis of mature root region, forming an efficient uptake system with OsLsi1 polarly localized at the distal side of the same cell layers. Expression of *OsBOR1* and *OsLsi1* was unaffected by B deficiency and excess. However, although OsLsi1 protein did not respond to high B at the protein level, OsBOR1 was degraded in response to high B within hours, which was accompanied with a significant decrease of total B uptake. The high B-induced degradation of OsBOR1 was inhibited in the presence of MG-132, a proteasome inhibitor, without disturbance of the polar localization. In contrast, neither the high B-induced degradation of OsBOR1 nor its polarity was affected by induced expression of dominant-negative mutated dynamin-related protein 1A (OsDRP1A^{K47A}) or knockout of the mu subunit (AP2M) of adaptor protein-2 complex, suggesting that clathrin-mediated endocytosis is not involved in OsBOR1 degradation and polar localization. These results indicate that, in contrast to *Arabidopsis thaliana*, rice has a distinct regulatory mechanism for B uptake through clathrin-independent degradation of OsBOR1 in response to high B.

Introduction

Boron (B) is essential for plant growth and development mainly through crosslinking two chains of pectin at rhamnogalacturonan II in the cell wall (Matoh, 1997; O'Neill et al., 2001). Therefore, B deficiency causes cessation of cell expansion in developing tissues such as the tips of roots and shoots, pollen, and other reproductive organs, resulting in stunting and distortion of the growing tip that can lead to tip death, brittle foliage, and sterility (Loomis and Durst, 1992; Dell and Huang, 1997; Marschner, 2012). On the other hand, high B is toxic to plants, causing symptoms such as

Received October 12, 2021. Accepted November 17, 2021. Advance access publication December 6, 2021

chlorosis, brownish leaf tips, and dark brown elliptical spots on leaves (Schnurbusch et al., 2010; Atique-ur-Rehman et al., 2018; Wu et al., 2019). Both B deficiency and toxicity cause crop losses in many areas of the world (Nable et al., 1997; Shorrocks, 1997; Matthes et al., 2020). The range between B deficiency and toxicity is narrower than any other element (Eaton, 1944), while B in soils is largely variable from deficient to toxic levels depending on soil types and growth environments. Therefore, to maintain an optimal internal B level, plants need to deal with B fluctuations by regulating uptake, root-to-shoot translocation, and distribution processes (Yamaji and Ma, 2021).

Soluble B in soil with a pH < 8 is present in the form of uncharged boric acid (H_3BO_3). Its uptake requires cooperation of two different types of transporters. In *Arabidopsis thaliana*, Nodulin 26 (NOD26)-like intrinsic protein 5;1 (AtNIP5;1) and B transporter 1 (AtBOR1) are involved in B uptake. AtNIP5;1 belongs to NOD26-like Intrinsic Protein (NIP) subfamily of aquaporin and is permeable to H_3BO_3 (Takano et al., 2006). It is polarly localized at the distal side (facing soil side) and responsible for transporting B from soil solution to the root cells. On the other hand, AtBOR1 is a B efflux transporter belonging to the BOR transporter family, which is conserved in plant and yeast (Yoshinari and Takano, 2017). In contrast to AtNIP5;1, AtBOR1 is polarly localized at the proximal side (facing stele side) of the root cells and responsible for exporting B from the cells toward the stele (Takano et al., 2002). Therefore, AtNIP5;1 and AtBOR1 form a directional pathway for radial transport of B in the roots (Yoshinari and Takano, 2017), which is necessary for efficient B uptake (Wang et al., 2017; Yoshinari et al., 2019).

In rice (*Oryza sativa*), B uptake by the roots is mediated by OsLsi1/OsNIP2;1 and OsBOR1. OsLsi1 also belongs to NIP subfamily, but is categorized in a different subgroup from AtNIP5;1 (Ma et al., 2006; Mitani et al., 2008). OsLsi1 is originally identified as a channel-type transporter for silicic acid (H_4SiO_4; Ma et al., 2006), but it is also permeable to H_3BO_3 (Mitani et al., 2008; Schnurbusch et al., 2010). OsLsi1 is localized at the distal side of exodermis and endodermis of rice roots (Ma et al., 2006). Physiological analysis with mutant showed that OsLsi1 rather than OsNIP3;1, a putative ortholog of AtNIP5;1, is a major transporter for B uptake in rice (Shao et al., 2018). Knockout of *OsLsi1* resulted in a significant decrease of B uptake and showed typical B-deficiency symptom under low B condition (Shao et al., 2018). On the other hand, OsBOR1 is a close homolog of AtBOR1 and functions as a B efflux transporter (Nakagawa et al., 2007). However, it is unknown whether OsLsi1 and OsBOR1 also form a cooperative system for B uptake in rice roots because the polarity of OsBOR1 in roots is unknown, although it was recently reported to be polarly localized in the node and leaf sheath (Shao et al., 2021). Homologs of AtNIP5;1 and AtBOR1 have also been functionally characterized in other plant species such as maize (*Zea mays*), barley (*Hordeum vulgare*), wheat (*Triticum aestivum*), and *Brassica napus* (Sutton et al., 2007; Schnurbusch et al., 2010; Chatterjee et al., 2014; Durbak et al., 2014; Pallotta et al., 2014; Zhang et al., 2017). Some of them show similar roles as AtNIP5;1 and AtBOR1. For example, Tassel-less 1 (AtNIP5;1 putative ortholog) and Rotten ear (AtBOR1 putative ortholog) are required for B uptake in maize (Chatterjee et al., 2014; Leonard et al., 2014).

There have been recent advances in the understanding of B transporter regulation in Arabidopsis (Yoshinari and Takano, 2017). At the transcriptional level, the expression of *AtNIP5;1* mRNA in the roots is upregulated by B deficiency (Takano et al., 2006), but downregulated by high B via post-transcriptional regulation (Tanaka et al., 2011). This downregulation is controlled by a minimum upstream open reading frame (uORF), AUGUAA, in the 5′-untranslated region of the mRNA. Higher B conditions enhance ribosome stalling at the AUG-stop and lead to suppression of translation and mRNA degradation (Tanaka et al., 2016). In contrast, AtBOR1 is mainly regulated at the protein level, but not at the transcriptional level. Upon exposure to high B concentration, AtBOR1 is ubiquitinated, followed by rapid internalization from plasma membrane to endosome via clathrin-mediated endocytosis (CME) and subsequent degradation in vacuoles (Takano et al., 2005; Kasai et al., 2011; Yoshinari et al., 2016, 2021). In addition, uORF-dependent translation suppression was also found in AtBOR1 at very high B condition (Aibara et al., 2018). However, the mechanisms for regulating transporters involved in B uptake in other plant species, such as rice, are still poorly understood.

Rice (*O. sativa*) is an important staple food and has a low requirement for B (Mengel and Kirkby, 1987; Blevins and Lukaszewski, 1998); it requires 5–10 mg/kg dry weight B in contrast to 20–70 mg/kg dry weight for most dicots (Marschner, 2012; Onuh and Miwa, 2021). Furthermore, the concentration of B in soil solution fluctuates greatly due to frequent soil water changes during growth period of rice. In addition, rice has a unique root anatomy. These distinct features of rice led us to hypothesize that rice has a different regulation mechanism for B uptake to cope with B fluctuations in soil (Yamaji and Ma, 2021). In this study, we investigated the transcriptional and posttranslational levels of OsLsi1 and OsBOR1 in response to B fluctuations and revealed distinct mechanisms for regulation of B uptake in rice roots.

Results

Polar localization of OsBOR1 in rice roots

OsLsi1 is localized at the distal side of both root exodermis and endodermis in rice (Ma et al., 2006), but it is unknown whether OsBOR1 also shows polarity. To observe the OsBOR1 polarity and compare it with OsLsi1 in the same roots under the same conditions, we generated a transgenic line carrying *Flag-OsLsi1* under the control of *OsLsi1* promoter in *lsi1* mutant background and performed double staining with antibodies against OsBOR1 and Flag, which were raised in different host animals. Introduction of

Flag-Lsi1 into *lsi1* mutant completely complemented its silicon (Si) uptake (Supplemental Figure S1), indicating that this construct is functional.

Rice root system consists of main roots including one seminal root and numerous crown roots, lateral roots including small and large lateral roots, and root hairs on main and lateral roots (Rebouillat et al., 2009; Coudert et al., 2010). In the root tip region of crown roots, OsBOR1 was localized at all cells except some parts of epidermis, but OsLsi1 signal was not detected (Figure 1A), which is consistent with very low expression of *OsLsi1* in this region reported in a previous study (Yamaji and Ma, 2007). OsBOR1 showed polar localization at the proximal side (Figure 1, B and C). In the mature region of crown roots, large and small lateral roots, similar to Flag-OsLsi1 (as OsLsi1 thereafter, green color; Ma et al., 2006; Yamaji and Ma, 2007), OsBOR1 (magenta color) was also localized at the exodermis and endodermis (Figure 1, D–H). OsBOR1 also showed polar localization, but in contrast to OsLsi1, OsBOR1 was polarly localized at the proximal side of plasma membrane in these roots (Figure 1, D–H). No signal was detected in the *OsBOR1* knockout mutant (*bor1-1*; Figure 1I), confirming the specificity of these antibodies against OsBOR1 and Flag.

Response of *OsLsi1* and *OsBOR1* expression to different B concentrations in rice roots

We further investigated the expression pattern of *OsBOR1* as well as of *OsLsi1* for comparison in the same roots in dose- and time-dependent manners. Consistent with previous results (Shao et al., 2018), the expression of *OsLsi1* did not respond to B either in dose- or time-dependent

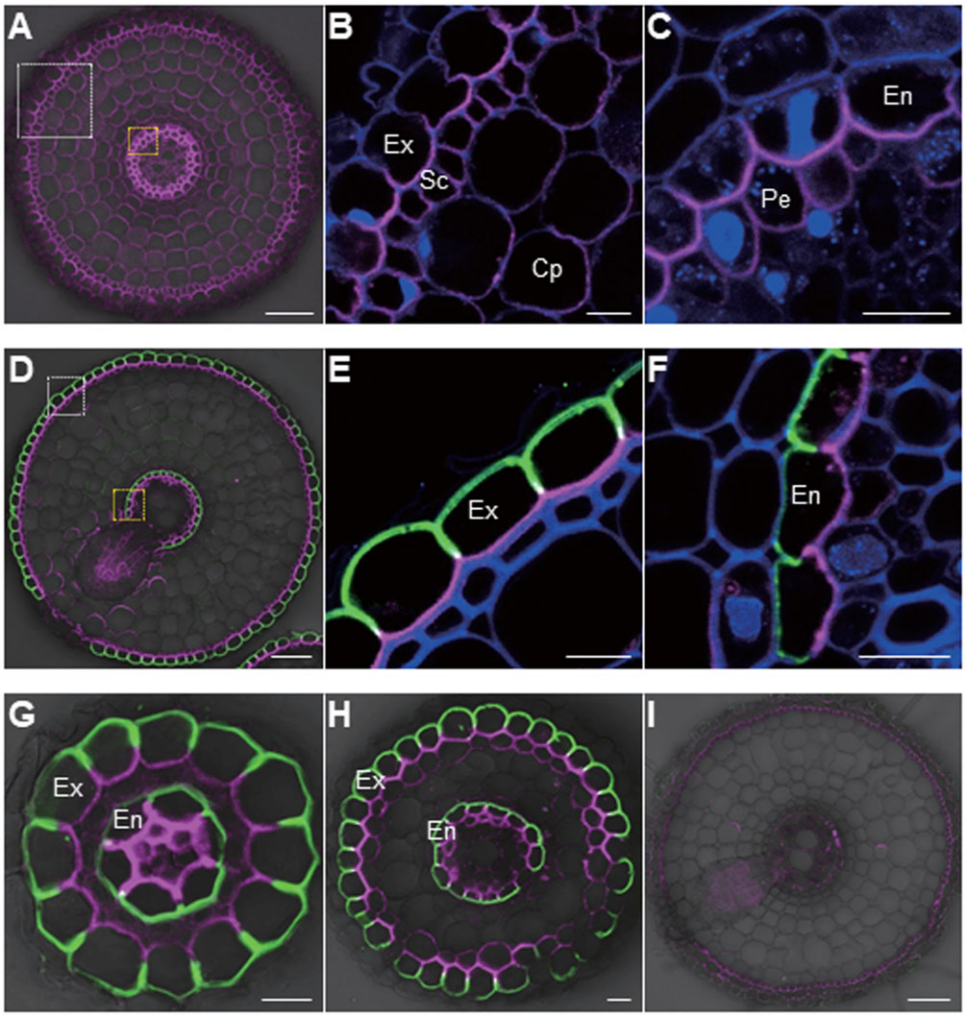

Figure 1 Polar localization of OsBOR1 and OsLsi1 in rice roots. A–H, Localization of OsBOR1 and OsLsi1 in root tip (A–C), mature root region of crown root (D–F), small (G), and large (H) lateral roots of transgenic line carrying functional *Flag-OsLsi1*. I, Localization of OsBOR1 and Flag-OsLsi1 in crown root of *bor1-1* mutant. White or yellow-dotted areas in (A) and (D) were enlarged in (B and E) or (C and F), respectively. Seedlings (25-d-old) precultured in a solution without B for 3 d were used for sampling the root tip (3 mm from the root tip) and mature region (15 mm) of crown roots, and lateral roots. Double immunostaining of OsBOR1 and Flag-OsLsi1 was performed. Magenta color shows the signal from OsBOR1, green color shows the signal from Flag-OsLsi1, and blue color from cell wall autofluorescence. Exodermis (Ex), sclerenchyma (Sc), cortex parenchyma (Cp), endodermis (En), and pericycle (Pe) are shown. Scale bars = 10 μm except (A, D, and I), which are 50 μm.

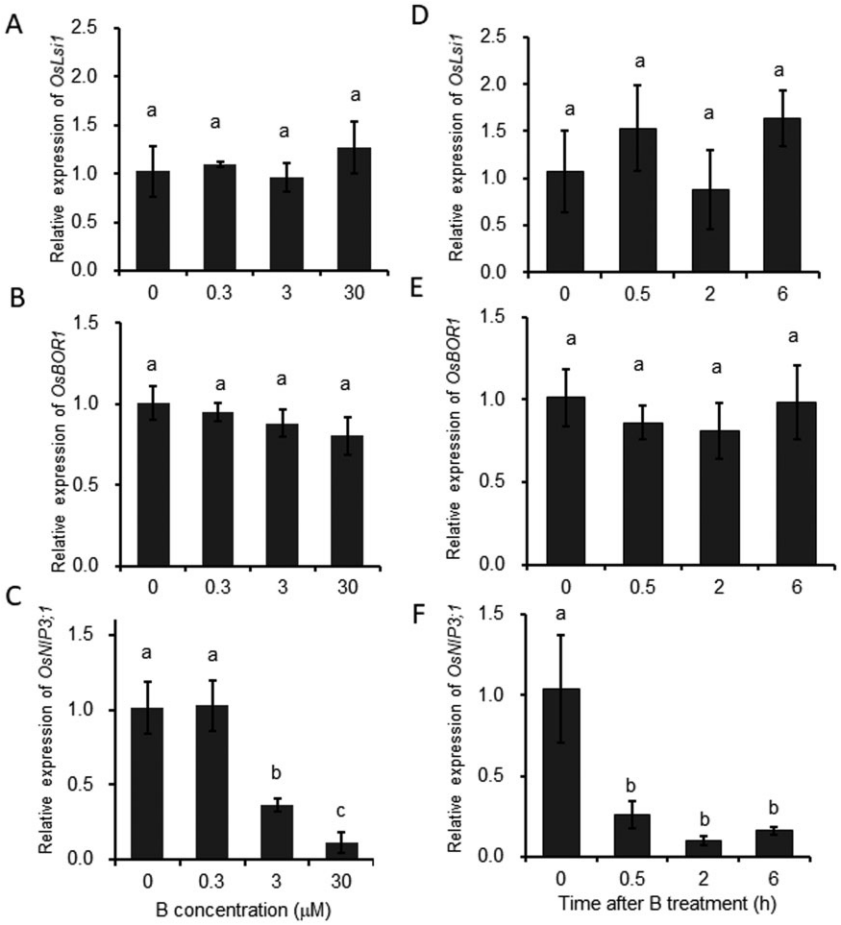

Figure 2 Dose- and time-dependent response of expression of *OsLsi1* and *OsBOR1* to different B concentrations in rice roots. A–C, Dose–response of *OsLsi1* (A), *OsBOR1* (B), and *OsNIP3;1* (C) expression in the roots. D–F, Time-dependent expression of *OsLsi1* (D), *OsBOR1* (E), and *OsNIP3;1* (F) in the roots in response to high B. For dose–response experiment, seedlings (21-d-old) were exposed to a solution containing 0, 0.3, 3, or 30 μM B for 7 d (A–C). For time-course experiment, seedlings (25-d-old) precultured in B-free solution for 3 d were exposed to 30 μM B for different times indicated (D–F). *OsNIP3;1* was used as a B-responsive marker gene (C and F). The expression level was determined by quantitative RT-PCR. *Histone H3* was used as an internal standard. Expression relative to the roots (−B) is shown. Data are means ± SD ($n = 4$). Different lowercase letters indicate significant difference at $P < 0.01$ by Tukey–Kramer's test.

manner (Figure 2, A and D). Similarly, the expression of *OsBOR1* was also not changed when the plants were exposed to a solution containing different B concentrations from 0 to 30 μM for 7 d (Figure 2B). Furthermore, a time-course experiment showed that when −B plants were exposed to a solution containing 30 μM B for different times, no significant change in the expression of *OsBOR1* was observed at all sampled time points (Figure 2E). These results indicate that both *OsLsi1* and *OsBOR1* are constitutively expressed in the roots. In contrast, the expression of *OsNIP3;1*, a B-responsive marker gene (Shao et al., 2018), was downregulated by high B in a dose- and time-dependent manner (Figure 2, C and F).

We also investigated the spatial expression pattern of *OsBOR1* in the roots. The results showed that the expression of *OsBOR1* was higher in the root mature region (1–2 cm from the root tip) than the root tip region (0–0.5 cm) (Supplemental Figure S2).

Response of OsLsi1 and OsBOR1 proteins to external B concentrations

To investigate the responses of OsBOR1 and OsLsi1 proteins to different B concentrations, we performed double immunostaining in a transgenic line carrying *Flag-OsLsi1*. At both the root tip (3 mm from the root tip) and mature region (15 mm) of the crown root, the signal of OsBOR1 (magenta color) was decreased with increasing B concentrations in the external solution (Figure 3, A–D and I), although the signal could be still detected at 30 μM B concentration. In contrast, the signal intensity of OsLsi1 was hardly affected by external B concentrations at the mature root region (Figure 3, E–H and J). The cell specificity of localization and polarity of both OsLsi1 and OsBOR1 were not altered by B concentrations (Figure 3, A–H).

To confirm high B-induced degradation of OsBOR1, we performed a western blot analysis. A major band was detected around 74 kDa, which corresponds to the

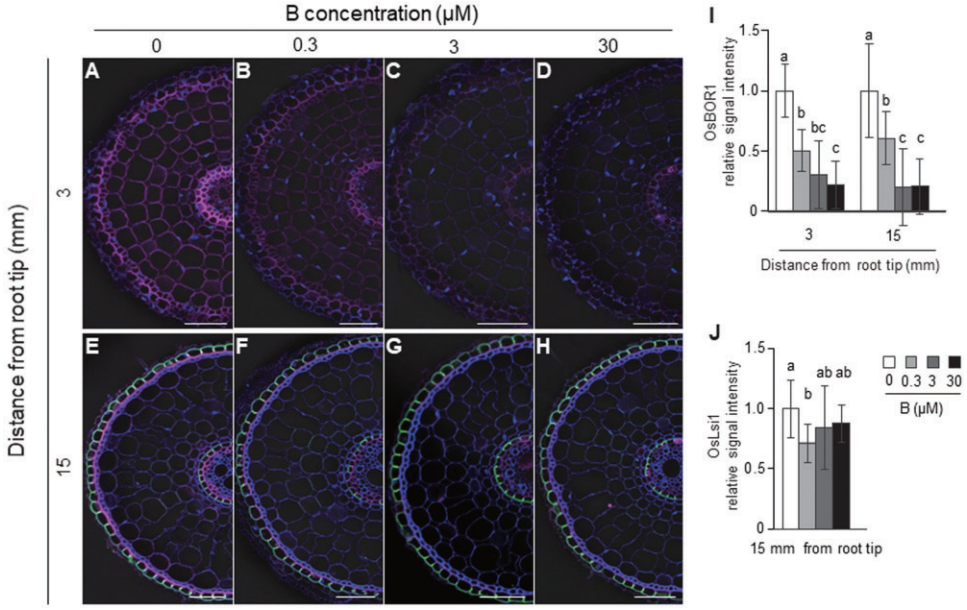

Figure 3 Effect of different B concentrations on localization and abundance of OsBOR1 and OsLsi1 proteins in rice roots. A–H, Localization of OsBOR1 and OsLsi1 in the root tip (A–D) and mature region (E–H) of crown roots. I and J, Signal intensity of OsBOR1 (I) and OsLsi1 (J). Transgenic seedlings (21-d-old) harboring *Flag-OsLsi1* were pretreated with −B for 3 d, followed by exposing to 0, 0.3, 3, or 30 μM B for 6 h. The root tip region (3 mm from root tip) and mature root region (15 mm) of crown roots were sampled for double immunostaining of OsBOR1 and Flag-OsLsi1. Magenta color shows signal from OsBOR1, green color shows signal from Flag-OsLsi1, and blue color from cell wall autofluorescence and nuclei staind by DAPI. Scale bars indicate 50 μm. The signal intensities of OsBOR1 and OsLsi1 were quantified by LAS AF Lite software and the intensity relative to −B condition is shown. All pictures were taken under the same conditions. Data are means ± SD (n = 9–16). Different letters indicate significant differences at $P < 0.05$ by Tukey–Kramer's test.

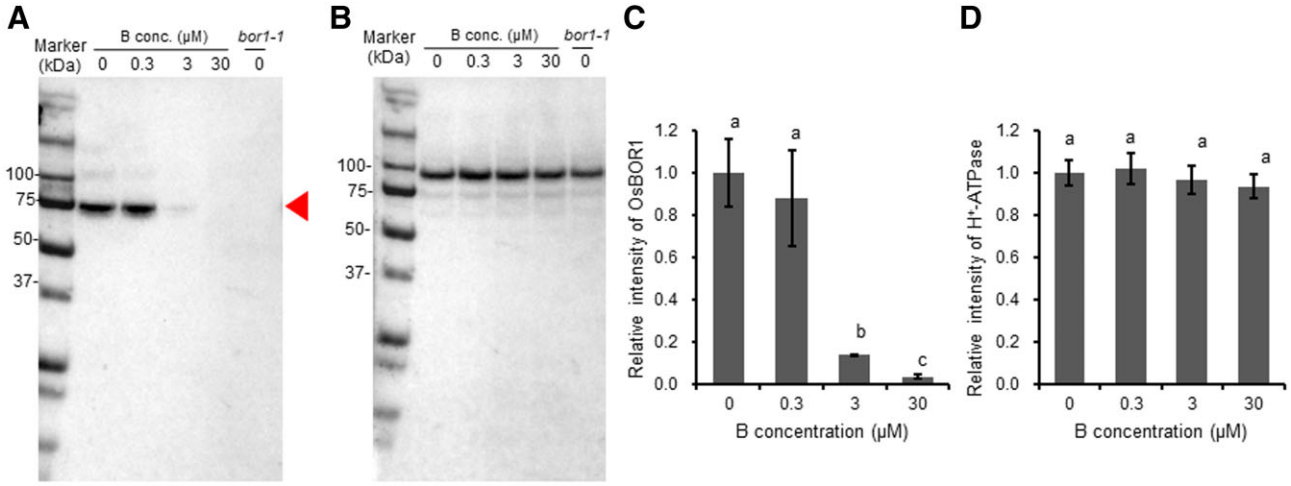

Figure 4 Western blot analysis of OsBOR1 protein in response to different B concentrations in rice roots. A and B, Western blot analysis of OsBOR1 (A) and H^+-ATPase (B) in response to different B concentrations. Red arrow shows the size of OsBOR1. C and D, Signal intensity of OsBOR1 (C) and H^+-ATPase (D). Seedlings (21-d-old) were exposed to 0, 0.3, 3, 30 μM B for 7 d. Roots were harvested for western blot analysis with three biological replicates. The microsome fraction was analyzed by SDS–PAGE and visualized by western blot with antibodies against OsBOR1 and H^+-ATPase (as an internal standard). Signal intensity of target band was quantified by Image Lab Software (Bio-Rad, Hercules, CA, USA) and the intensity relative to −B is shown. Data are means ± SD (n = 3). Left lane shows molecular weight markers. Different lowercase letters indicate the significant difference at $P < 0.01$ by Tukey–Kramer's test.

estimated molecular weight of OsBOR1 (Figure 4A). Similar to the immunostaining results (Figure 3), the protein abundance of OsBOR1 was decreased with increasing B concentrations except for 0.3 μM B (Figure 4, A and C). In contrast, the abundance of H^+-ATPase as a control was not altered by B concentrations (Figure 4, B and D).

To investigate the speed of OsBOR1 degradation in response to high B, we performed a time-course experiment.

When −B plants were exposed to a high B (30 μM) solution, the OsBOR1 signal intensity was not altered at 0.5 h after the B exposure, but decreased at 2 h and thereafter at both the root tip and mature root region of the crown roots (Figure 5, A–F and M). In contrast, the signal intensity of OsLsi1 in the mature root region was not altered by high B supply at any time points (Figure 5, G–L and N). These results were confirmed by western blot analysis (Supplemental Figure S3, A–C). These findings indicate that OsBOR1 protein, but not OsLsi1 was degraded in response to high B concentrations.

We also investigated the response of OsBOR1 protein to B-deficiency by transferring + B plants to a solution free of B. The signal of OsBOR1 in the roots was weakly observed in B-sufficient plants (Figure 6A), but was greatly enhanced after exposure to B-free solution for 1 and longer time (Figure 6, B–E).

Effect of protein synthesis inhibitor on high B-induced degradation of OsBOR1

To examine whether the high B-induced degradation of OsBOR1 results from translational repression, we exposed the roots to cycloheximide (CHX), a protein synthesis inhibitor, and compared the change of OsBOR1 abundance in the absence and presence of high B. In the absence of B, OsBOR1 abundance was decreased by treatment with CHX (Supplemental Figure S4), suggesting that OsBOR1 synthesis was inhibited and CHX treatment is effective. In the presence of high B without CHX, the degradation of OsBOR1 was observed (Supplemental Figure S4). However, in the presence of high B and CHX, the degradation of OsBOR1 was also observed (Supplemental Figure S4). This result suggests that the high B-induced OsBOR1 degradation is not caused by translational repression.

CME is not involved in the high B-induced degradation and polarity of OsBOR1

In Arabidopsis, CME has been reported to be involved in B-induced degradation and polar localization of AtBOR1 (Takano et al., 2010; Kasai et al., 2011; Yoshinari et al., 2016, 2019), and adaptor protein 2 (AP-2) complex-dependent CME is crucial for the polar localization of AtBOR1 (Yoshinari et al., 2019). The AP-2 complex is a heterotetramer consisting of two large adaptins (alpha and beta), a medium adaptin (mu), and a small adaptin (sigma), and is responsible for cargo selection and clathrin recruitment of part of CME (Zhang et al., 2015).

We first investigated whether AP-2-dependent CME is involved in polar localization and B-induced degradation of OsBOR1 in rice. For this purpose, we generated knockout lines of the *OsAP2M* gene, which encodes the mu subunit.

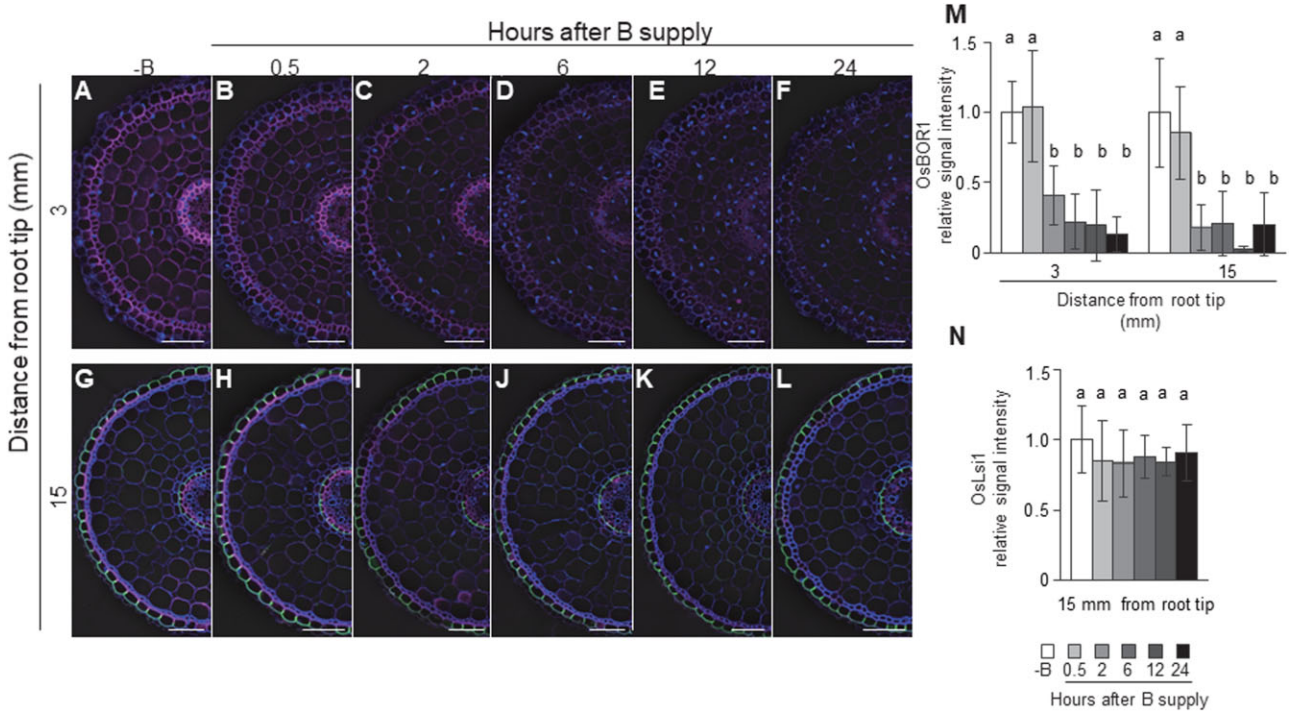

Figure 5 Time-dependent response of OsBOR1 and OsLsi1 proteins to high B supply in rice roots. A–L, Localization of OsBOR1 and OsLsi1 in the root tip (A–F) and mature region (G–L) of crown root. M and N, Signal intensity of OsBOR1 (M) and OsLsi1 (N). Transgenic seedlings (21-d-old) harboring *Flag-OsLsi1* were precultured in a solution free of B (−B) for 3 d and then transferred to a solution containing 30 μM B. At different time points including 0.5, 2, 6, 12, and 24 h, tip region (3 mm from root tip) and mature region (15 mm) of crown roots were sampled for double immunostaining of OsBOR1 and Flag-OsLsi1. Magenta color shows signal from OsBOR1, green color shows signal from Flag-OsLsi1, and blue color from cell wall autofluorescence and nuclei staind by DAPI. Scale bars indicate 50 μm. The signal intensities of OsBOR1 and OsLsi1 were quantified by LAS AF Lite software and the intensity relative to −B condition is shown. All pictures were taken under the same conditions. Data are means ± SD (n = 8–16). Different letters indicate significant differences at $P < 0.05$ by Tukey–Kramer's test.

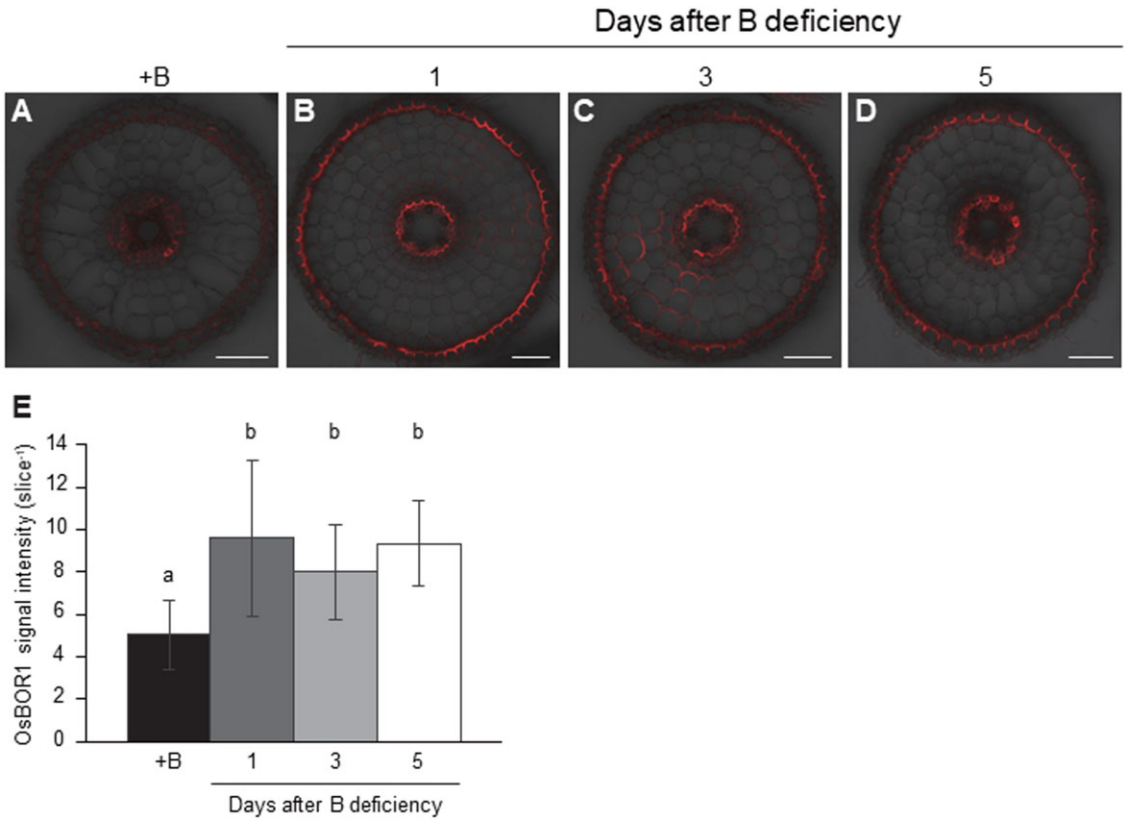

Figure 6 Time-dependent response of OsBOR1 to B-deficiency in rice roots. A–D, Localization of OsBOR1 at 0 (A), 1 (B), 3 (C), and 5 (D) days after B-deficiency. E, Signal intensity of OsBOR1. Seedlings (25-d-old) were precultured in a solution containing 30 μM B for 3 d and then transferred to a solution free of B for 0, 1, 3, and 5 d. Mature region (15 mm) of crown roots were sampled for immunostaining of OsBOR1. Red color shows signal from OsBOR1. Signals were merged with bright field. Scale bars = 50 μm. All pictures were taken under the same conditions. The signal intensities of OsBOR1 were quantified by LAS AF Lite software. Data are means ± SD (n = 10–15). Different letters indicate significant differences at $P < 0.05$ by Tukey–Kramer's test.

However, unlike AtBOR1, the cellular localization, polarity, and protein abundance of OsBOR1 in roots were not affected by *OsAP2M* knockout in the −B plants (Supplemental Figure S5, A and C). Furthermore, exposure to 30 μM B for 6 h similarly resulted in the degradation of OsBOR1 in lines with or without functional AP-2 (Supplemental Figure S5, B and D). These results suggest that the AP-2-dependent CME is not involved in OsBOR1 polarity and degradation in rice roots.

We then used an estradiol inducible expression system expressing the mutated dynamin-related protein1A (DRP1A) to investigate the involvement of the entire CME pathway in the polar localization and degradation of OsBOR1. DRP1A is an essential protein for CME to cut off the clathrin-courted vesicle from the plasma membrane (Zhang et al., 2015). Since the K47 residue is required for GTP binding, substitution K47 to A results in loss of function of AtDRP1A in Arabidopsis (Yoshinari et al., 2016). When *mRFP*-tagged *AtDRP1A*^{K47A} is introduced under an estradiol inducible promoter, AtDRP1A^{K47A} could inhibit CME in a dominant-negative manner only after estradiol supply (Yoshinari et al., 2016). In the case of AtBOR1 in Arabidopsis root, when the entire CME pathway was inhibited by AtDRP1A^{K47A}, both polar localization and B-induced degradation were inhibited (Yoshinari et al., 2016). Since K47 is conserved in OsDRP1A of rice, we, therefore, generated transgenic rice lines carrying K47A mutated *OsDRP1A* fused with hemagglutinin (HA)-tag (OsDRP1A^{K47A}-HA) under the control of an estradiol-inducible promoter.

First, to test whether the endocytosis was inhibited by the induction of *OsDRP1A*^{K47A}*-HA*, we fed FM4–64, an endocytic tracer, to the roots and observed its internalization. In the absence of OsDRP1A^{K47A}-HA expression, FM4–64 was actively taken up into the root cells of the transgenic line (Supplemental Figure S6A). However, when the OsDRP1A^{K47A}-HA was induced by estradiol, the uptake of FM4–64 was significantly suppressed (Supplemental Figure S6, B and G). As a control, FM4–64 uptake was also investigated in the nontransgenic wild-type (WT) rice (cv. Nipponbare) in the presence of estradiol. The result showed that the active uptake of FM4–64 was also observed (Supplemental Figure S6, C and G). Immunostaining with HA antibody showed that the signal was only detected in the transgenic plants induced by estradiol (Supplemental

Figure S6, D–F). These results indicate that OsDRP1A^{K47A}-HA could inhibit CME in rice.

By using the same plants, we then investigated the response of OsBOR1 to high B (30 μM B) in the presence and absence of estradiol. Results showed that OsBOR1 protein signal was significantly reduced by exposure to high B for 6 h in the absence of estradiol in both the root tip (Figure 7, A, B, and Q) and mature root region of the crown roots (Figure 7, I, J, and Q). However, induction of *OsDRP1A^{K47A}-HA* expression by estradiol did not inhibit the degradation of OsBOR1 (Figure 7, C–D, K–L, and Q), although the expression of *OsDRP1A^{K47A}-HA* was induced, which was confirmed by immunostaining using HA antibody (Figure 7, E–H, M–P, and R).

We further compared OsBOR1 signal intensity between cells with high and low induction of OsDRP1A^{K47A}-HA in the roots with low induction after exposure to high B for 6 h (Supplemental Figure S7A). When signal intensity of OsBOR1 and OsDRP1A^{K47A}-HA was quantified in each cell (Supplemental Figure S7E), the OsBOR1 abundance was similar in cells with high and low accumulation of OsDRP1A^{K47A}-HA (Supplemental Figure S7, B–D and F–G). Furthermore, the polar localization of OsBOR1 was also not altered by induction of OsDRP1A^{K47A}-HA (Supplemental Figure S7, B–D). These results, together with AP-2 mutant results, indicate that CME is not involved in the protein degradation and polarity of OsBOR1 in rice.

We further investigated the effect of Brefeldin A (BFA) on OsBOR1 degradation. BFA is able to inhibit the exocytosis of plasma membrane proteins during protein recycling (Geldner et al., 2001). Since BFA inhibits only exocytosis but not endocytosis, treatment with BFA results in accumulation of AtBOR1 in the intracellular region, which is called the BFA body (Takano et al., 2005: Yoshinari et al., 2019). We, therefore, observed whether the BFA body was formed in the presence of BFA in rice roots. However, unlike AtBOR1, no clear BFA body was observed after BFA treatment in both the root tip and mature root region (Supplemental Figure S8).

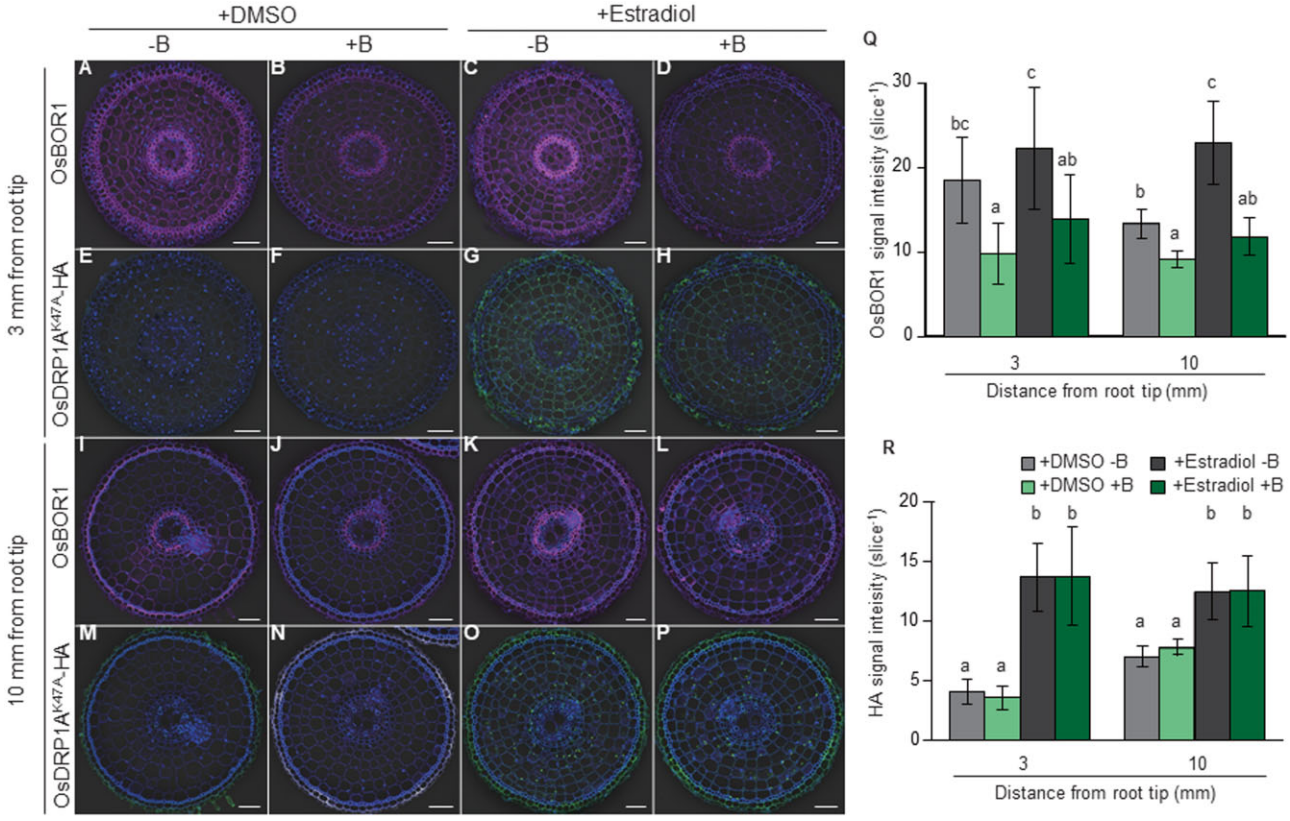

Figure 7 Effect of mutated dynamin-related protein1A (OsDRP1A^{K47A}) induction on degradation and polarity of OsBOR1 in rice roots. A–P, Localization of OsBOR1 (A–D and I–L) and OsDRP1A^{K47A}-HA (E–H and M–P) in root tip (A–H) and mature region (I–P) of crown roots. (Q and R) Signal intensity of OsBOR1 (Q) and OsDRP1A^{K47A}-HA (R). Transgenic seedlings (21-d-old) harboring *Est≫OsDRP1A^{K47A}-HA* were treated −B for 1 d, followed by exposing to −B solution containing DMSO (as a control) or 20 μM β-estradiol for 2 d. Subsequently, these seedlings were exposed to 0 or 30 μM B in the presence of DMSO or 20 μM β-estradiol. After 6 h, tip region (3 mm from root tip) and mature region (10 mm) of crown roots were sampled for double immunostaining of OsBOR1 and OsDRP1A^{K47A}-HA. Magenta and green signals indicate OsBOR1 and OsDRP1A^{K47A}-HA, respectively. Blue signals indicate autofluorescence of the cell wall and DAPI-stained nucleus. Signal of OsBOR1 or OsDRP1A^{K47A}-HA were merged with bright field and autofluorescence of the cell wall and DAPI-stained nucleus. Scale bars indicate 50 μm. Signal intensities of OsDRP1A^{K47A}-HA and OsBOR1 were quantified by LAS AF Lite software. All pictures were taken under the same conditions. Data are means ± SD (n = 6–10). Different letters indicate significant differences at $P < 0.05$ by Tukey–Kramer's test.

Effect of lytic vacuolar and proteasome inhibitors on high B-induced degradation of OsBOR1

In Arabidopsis roots carrying *AtBOR1-GFP*, GFP signal could be observed in vacuoles in the presence of concanamycin A (ConcA), a specific inhibitor of vacuolar-type H^+-ATPase activity and high B, indicating inhibition of the lytic vacuole activity (Takano et al., 2005). We then tested the effect of ConcA, on the high B-induced degradation of OsBOR1. However, no OsBOR1 signal was observed in vacuoles after high B and ConcA treatments, although its signal intensity at the plasma membrane was suppressed by high B supply in the presence and absence of ConcA in both the root tip and root mature region (Supplemental Figure S9).

Since previous studies showed that degradation of some mineral transporters relied on proteasome-dependent pathway in plants (Shin et al., 2013; Park et al., 2014; Li et al., 2020), we, therefore, sought to determine if the proteasome-dependent pathway is involved in the B-induced OsBOR1 degradation by immunostaining and western blot analysis. To investigate this, we exposed −B plants to a solution containing 0 or 30 μM B in the presence or absence of MG-132, a proteasome inhibitor (Adams and Stein, 1996). In the absence of MG-132 (DMSO), OsBOR1 was degraded by high B (Supplemental Figure S10, A, B, and E). However, in the presence of MG-132, OsBOR1 degradation by B was inhibited (Supplemental Figure S10, C–E). This result was also confirmed by western blot analysis (Supplemental Figure S10F). All these results suggest that proteasomal degradation is one of the mechanisms involved in the high B-induced degradation of OsBOR1.

OsBOR1-degradation decreases B uptake

To associate OsBOR1-degradation with B uptake, we performed a short-term labeling experiment with stable B isotopes; ^{11}B and ^{10}B. To do this experiment, we first grew the WT and two mutants of *OsBOR1* in a nutrient solution containing 30 μM ^{11}B, followed by exposure to a solution with or without 30 μM ^{11}B for 3 d. These plants were then exposed to a solution containing 0.3 μM or 30 μM ^{10}B for 10 h. Three-day treatment with B-deficiency hardly affected the growth of both the roots and shoots (Supplemental Figure S11). The ^{10}B uptake normalized by root biomass during the 10 h treatment was significantly decreased in WT pretreated with 30 μM ^{11}B compared to pretreated without B at both 0.3and 30 μM ^{10}B (Figure 8, A and B). However, this decrease was not significant or very small in two mutants (Figure 8, A and B). The ^{10}B uptake was significantly lower in two mutants than in the WT, irrespective of B pretreatment (Figure 8, A and B), confirming the important role of OsBOR1 in B uptake. These results also indicate that high B-induced degradation of OsBOR1 plays an important role in shutting down B uptake in response to high B. Since OsBOR1 was not completely degraded at 30 μM B (Figure 2), this may explain the difference in ^{10}B uptake between WT and mutants at this concentration (Figure 8, A and B).

We also compared the root-to-shoot translocation of ^{10}B between WT and two mutants. Slight difference (2%–4% difference) in the root-to-shoot translocation ratio of ^{10}B was observed between WT and mutants, and between plants pretreated with or without ^{11}B at both 0.3 and 30 μM ^{10}B (Figure 8, C and D). These results indicate that OsBOR1 also slightly contributes to the root-to-shoot translocation of B in both B-deficient and sufficient plants.

Discussion

Uptake of B is mediated by OsLsi1 and OsBOR1 in rice roots (Nakagawa et al., 2007; Shao et al., 2018). Through detailed analysis of these two transporters in rice, we uncovered a B uptake system with a regulatory mechanism distinct from that in Arabidopsis.

Polarly localized-OsBOR1 cooperatively works with OsLsi1 for efficient B uptake in the roots

Mature roots of rice are characterized by a distinct anatomy; two Casparian strips at the exodermis and endodermis and formation of highly developed aerenchyma between the exodermis and endodermis (Enstone et al., 2002). Therefore, uptake of a mineral element requires the cooperation of both influx (or channel) and efflux transporters localized at the exodermis and endodermis (Sasaki et al., 2016; Che et al., 2018; Mitani-Ueno et al., 2018; Huang et al., 2020; Yamaji and Ma, 2021). Such cooperative uptake systems for Si and manganese (Mn) have been elucidated in rice roots. Si uptake is mediated by OsLsi1 and OsLsi2 (Ma et al., 2006, 2007), whereas Mn uptake is mediated by OsNramp5 and OsMTP9 (Sasaki et al., 2012; Ueno et al., 2015). OsLsi1 and OsNramp5 are polarly localized at the distal side of both exodermis and endodermis, while OsLsi2 and OsMTP9 are localized at the proximal side of the same cell layers as OsLsi1 and OsNramp5. Furthermore, our mathematical modeling indicated that such influx–efflux transporter combination is the most efficient for Si uptake (Sakurai et al., 2015). For B, its uptake has been proposed to be mediated by OsLsi1 and OsBOR1 in rice roots (Nakagawa et al., 2007; Shao et al., 2018). Although OsLsi1 shows polar localization, the polarity of OsBOR1 is unknown. In this study, we took advantage of double immunostaining of both OsBOR1 and OsLsi1 in transgenic line and clearly showed that OsBOR1 and OsLsi1 are localized at the same cell layers, but show different polarity. OsLsi1 is polarly localized at the distal side of both exodermis and endodermis, while OsBOR1 is polarly localized at the proximal side in both crown roots and lateral roots (Figure 1, D–H). These results indicate that OsLsi1 and OsBOR1 polarly localized at the same cells form a cooperative uptake system for B (Figure 9). That is, B is first imported into the symplast by OsLsi1 at the distal side of the exodermal cells and then exported by OsBOR1 at the proximal side to the apoplastic connections of aerenchyma (Figure 9). B is further imported into the symplast of the endodermis by OsLsi1 localized at the distal side, and exported

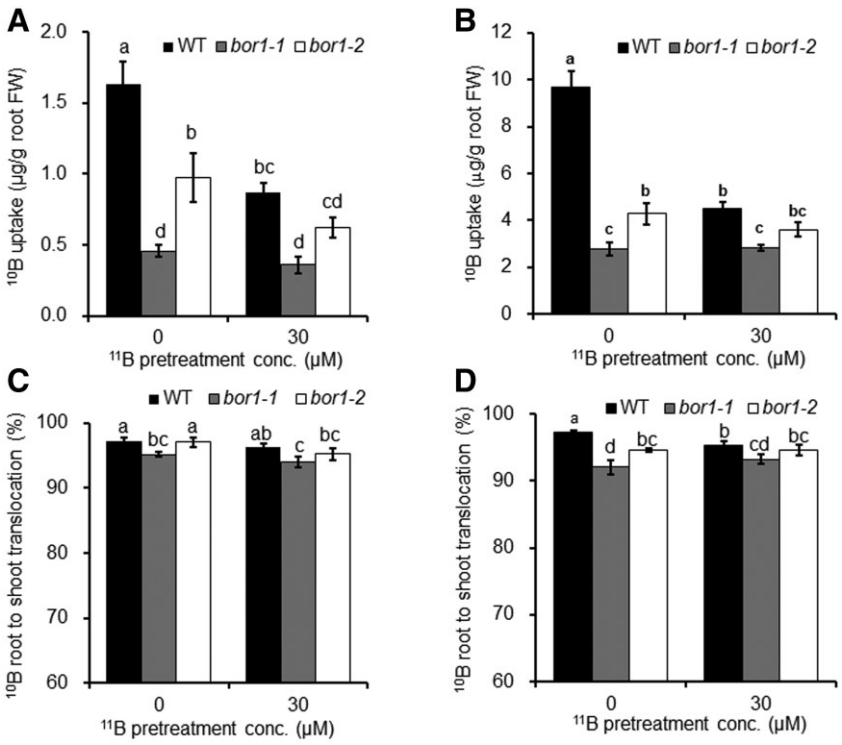

Figure 8 Effect of pretreatment with different B supply on short-term uptake and root-to-shoot translocation of B. A and B, Uptake, (C and D) root-to-shoot translocation of ^{10}B. Seedlings (20-d-old) precultured with 30 μM ^{11}B were exposed to a solution with or without 30 μM ^{11}B for 3 d. These plants were then exposed to a solution containing 0.3 μM (A and C) or 30 μM (B and D) ^{10}B for 10 h. Roots and shoots were separately harvested and subjected to determination of ^{10}B by inductively coupled plasma mass spectrometry with isotope mode. Data are means ± SD (n = 3). Different letters indicate significant differences at $P < 0.05$ by Tukey–Kramer's test.

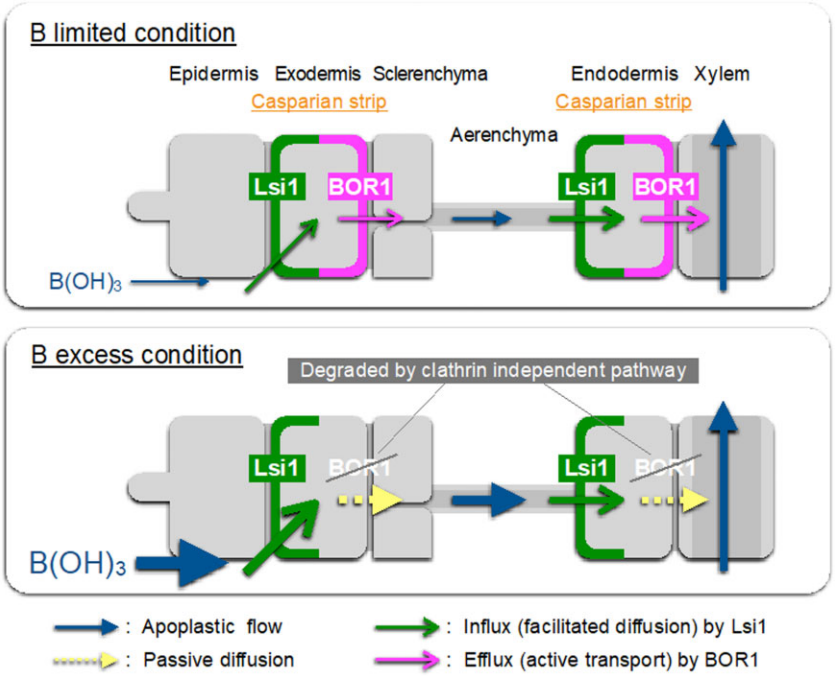

Figure 9 Schematic presentation for B uptake system and its regulation in rice roots. B uptake in rice roots is mediated by OsLsi1 and OsBOR1, which are polarly localized at the distal and proximal side of both exodermis and endodermis. OsLsi1 is not regulated at both transcriptional and posttranslational level, while OsBOR1 protein is degraded in response to high B concentrations through clathrin-independent pathway. Thickness of arrows roughly represents the contribution of each step.

to the stele by OsBOR1 localized at the proximal side of the endodermis for subsequent translocation to the shoots.

A previous study reported that OsBOR1 is strongly expressed in the stele, but only slightly in the exodermis and endodermis in roots of plants harboring the *OsBOR1* promoter fused with β-*glucuronidase* gene (*GUS*) under normal B condition, whereas it was expressed in the exodermis and stele in the roots under −B condition (Nakagawa et al., 2007). However, by using a specific antibody against OsBOR1 in this study, we found that OsBOR1 was localized mainly at the exodermis and endodermis, but not at the stele in the mature region of the roots exposed to −B condition (Figure 1, D–F). Furthermore, the cell specificity of OsBOR1 localization was not altered with change of external B concentrations (Figure 3). One possibility for this inconsistency could be attributed to artifacts of GUS fusion because the promoter activity was not confirmed. Therefore, OsBOR1 in root is primarily involved in B uptake. However, since B released by endodermis-localized OsBOR1 into the apoplastic space of root stele can also directly enter the xylem vessel, knockout of *OsBOR1* resulted in slight decrease in the root-to-shoot translocation of B (Figure 8). For efficient xylem loading of B, a transporter expressed at the pericycle may be required, which remains to be identified.

Distinct regulatory mechanisms of B uptake in rice

Our results showed that, in order to maintain B homeostasis under B fluctuations, rice has developed a regulatory mechanism for B uptake through finely regulating B transporters in the roots. OsLsi1 did not respond to low and high B at both transcript and protein levels (Figures 2 and 3; Shao et al., 2018). However, OsBOR1 protein was gradually decreased in response to high B, although the expression of *OsBOR1* is constitutive (Figures 2–5; Nakagawa et al., 2007). Conversely, when the plants were exposed to −B solution, OsBOR1 protein was increased after 1 d (Figure 6). These findings indicate that B uptake in rice roots is regulated by OsBOR1, rather than OsLsi1 in response to changing B concentrations (Figure 9). This is a reasonable regulation system because OsLsi1 is primarily responsible for Si uptake (Ma et al., 2006; Yamaji and Ma, 2021). When OsBOR1 protein is degraded in response to high B, the active transport of B from external solution to the root cells will also be stopped because OsLsi1 is a channel-type transporter, which is passively transported following the concentration gradient of B between external and internal B solution (Figure 9).

In Arabidopsis, B uptake is regulated by both AtNIP5;1 and AtBOR1 (Yoshinari and Takano, 2017). *AtNIP5;1* mRNA level is downregulated in response to high B to minimize excess B entry to the root cells (Tanaka et al., 2016), whereas AtBOR1 is mainly regulated at the protein level (Takano et al., 2010). Under high-B conditions, AtBOR1 is more frequently in the outward-open state, with the C-terminal region exposed, giving E3 ligases access to the K590 residue for ubiquitination (Yoshinari et al., 2021). After the ubiquitination, the protein undergoes internalization from plasma membrane to endosome, via AP-2-dependent CME pathway, and subsequent degradation in vacuoles (Yoshinari et al., 2019). This is supported by the finding that B-induced AtBOR1 degradation is blocked by inhibition of CME using an inducible expression system of the AtDRP1A^{K47A} variant in Arabidopsis (Yoshinari et al., 2016). However, our results in this study showed that, unlike AtBOR1, CME is not involved in the degradation of OsBOR1 in rice roots (Figure 7; Supplemental Figures S5 and S7). This is supported by several pieces of evidence; (1) the degradation was not inhibited by *OsAP2M* knockout and dominant-negative OsDRP1A^{K47A} induction (Figure 7; Supplemental Figures S5 and S7) and (2) unlike AtBOR1, the BFA body was not observed in OsBOR1 (Supplemental Figure S8). Clathrin-independent endocytosis, such as membrane microdomain-associated endocytosis via flotillin1, is a potential internalization process of OsBOR1 because this process was reported to be involved in internalization of brassinosteroid receptor BRI1 in Arabidopsis (Wang et al., 2015), but the exact mechanisms for the internalization process of OsBOR1 require further investigation.

Vacuolar degradation and the proteasomal degradation are two major protein degradation mechanisms in the eukaryote cells (Finley, 2009). In this study, we found that OsBOR1 degradation was inhibited by proteasome inhibiter MG-132, but not by lytic vacuolar inhibitor ConcA (Supplemental Figures S9 and S10). These results suggest the possibility that OsBOR1 degradation is mediated by proteasomes.

OsBOR1 was still localized at the plasma membrane in the presence of MG-132 and high B (Supplemental Figure S10). A similar phenomenon was also observed for the flagellin receptor FLS2 in Arabidopsis (Robatzek et al., 2006). There are three possible explanations for this result; 1) the internalization of OsBOR1 is blocked by MG-132 directly before proteasome degradation, 2) MG-132 indirectly inhibits the OsBOR1 internalization by disturbing the stability of cytosolic proteins involved in the maintenance/turnover of membrane proteins (Barberon et al., (2011), and 3) OsBOR1 degradation occurs at the plasma membrane. The third one was reported for yeast copper transporter, Ctr1p (Ooi et al., 1996), although this possibility is low because proteasome-dependent degradation typically occurs in the cytosol. The exact mechanisms underlying B-induced OsBOR1 degradation require further investigation. In addition, it seems that, in contrast to AtBOR1 (Aibara et al., 2018), the high B-induced degradation of OsBOR1 is not caused by translational repression because CHX did not affect the degradation of OsBOR1 (Supplemental Figure S4). Furthermore, in contrast to rapid degradation (within minutes) of AtBOR1 in response to high B (Takano et al., 2010), degradation of OsBOR1 is relatively slow (within hours) (Figure 5; Supplemental Figure S3). All these findings indicate that, in contrast to Arabidopsis, rice has developed a distinct regulatory mechanism for B uptake in the roots. This difference in the regulation may be attributed to different growth conditions, B requirement, and root

structure (anatomy). Rice is usually grown in a paddy field and has a low B requirement compared with Arabidopsis. Furthermore, the root structure of rice is largely different from Arabidopsis. It will be interesting to investigate if other plant species have a similar regulation mechanism to rice.

Polar localization of transporters is important for directional uptake of mineral elements in rice and Arabidopsis (Sakurai et al., 2015; Wang et al., 2017; Che et al., 2018; Yoshinari et al., 2019). It was reported in Arabidopsis that constitutive AP-2-dependent CME is required to maintain polar localization of both AtNIP5;1 and AtBOR1 (Wang et al., 2017; Yoshinari et al., 2019). However, the polar localization of OsBOR1 was maintained in *osap2m* knockout mutant and OsDRP1A^{K47A} induced cells (Figure 7; Supplemental Figures S5 and S7), suggesting that, unlike in Arabidopsis, CME is not required for the polar localization of OsBOR1 in rice. The exact mechanisms underlying the polarity of OsBOR1 and OsLsi1 need to be investigated in the future.

In addition to B uptake, it was recently reported that, in rice, distribution of B to different organs and tissues is also finely regulated depending on their requirements and environmental B levels (Shao et al., 2021). In contrast to the B uptake system, OsNIP3;1 and OsBOR1 form a cooperative system for B distribution in the nodes and leaves of rice (Yamaji and Ma, 2021). Furthermore, OsNIP3;1 is regulated at both transcriptional and protein levels in response to B fluctuations (Shao et al., 2018), whereas OsBOR1 is degraded by high B although its transcript is not affected (Shao et al., 2021). These findings indicate that rice has developed a sophisticated system for maintaining B homeostasis by regulating transporters involved in B uptake and other processes at the transcript and/or protein level.

Materials and methods

Plant materials and growth conditions

WT rice (*O. sativa*, cv. Nipponbare) and two *Tos-17* retrotransposon insertion mutant lines of *OsBOR1* (NC0170/*bor1-1* and NC0255/*bor1-2*) obtained from Rice Resource Center in Japan (https://tos.nias.affrc.go.jp/), transgenic lines prepared as described below, were used. *bor1-1* is a knockout line, whereas *bor1-2* is a mutant with decreased expression, but the mutated protein showed transport activity for B (Nakagawa et al., 2007). After the seeds were soaked in water for 2 d at 30°C in the dark, the germinated seeds were transferred onto nylon nets floating on a solution containing 0.5 mM $CaCl_2$ in a 1.2-L pot as described before (Ma et al., 2002). After 5 d, the seedlings were transferred to a half-strength Kimura B nutrient solution including freshly prepared 2 μM $FeSO_4$ (pH 5.6) and the solution was renewed every 2 d (Ma et al., 2001). All experiments were conducted in a closed greenhouse at 25–30°C under natural sunlight with at least three biological replicates.

Generation of transgenic lines

To generate transgenic rice carrying *Flag-OsLsi1* under the control of *OsLsi1* promoter, the promoter (2,000 bp) was amplified from rice genome using the following primers, Lsi1P_2k_F_XhoI: ACCTCGAGGAAACACCTCGTGAACG, Lsi 1P_2k_R_Hind3: ACAAGCTTTTCTGACGCTCTATCTAG. This PCR product was cloned into a pTA2 cloning vector (Toyobo, Osaka, Japan). Flag-tag was attached to the N-terminus of *OsLsi1* coding sequence (CDS) by overlap polymerase chain reaction (PCR) using previously generated plasmid as a template (Mitani-Ueno et al., 2011). First, OsLsi1 CDS was amplified by the following primers; Flag-Lsi1 F-TACAAGGACGACGATGACAAGATGGCCAGC and Lsi1cds_R_XbaI 2-ACTCTAGATTCACACTTGGATGTTCTC. Then, the PCR product was used for the template of the second PCR with primers; Hind3-Flag F-AAGCTTATGGACTACAA GGAC and Lsi1cds_R_XbaI. The second PCR product was cloned into a pTA2 cloning vector. *OsLsi1* promoter and *Flag-OsLsi1* were inserted into pPZP2H-lac vector using XhoI and HindIII or HindIII and XbaI restriction sites, respectively. *Nopaline synthase* terminator gene was inserted behind the *Flag-OsLsi1* using SacI restriction site of pPZP2H-lac vector. This construct was transformed into calluses of *lsi1* mutant (Chiba et al., 2009) by *Agrobacterium tumefaciens* mediated transformation (Hiei et al., 1994). To examine whether Flag-OsLsi1 is functional in *lsi1* mutant, we compared Si uptake among WT (cv. Nipponbare), *lsi1* knockout mutant, and transgenic line (T1) harboring *pOsLsi1::Flag-OsLsi1*. Seedlings (21-d-old) were exposed to a 0.5 mM Si as H_4SiO_4 for 6 h and the uptake was investigated according to Ma et al. (2002).

To generate transgenic lines carrying *Est≫OsDRP1A^{K47A}-HA*, the *OsDRP1A* (*Os05g0556100*) CDS was amplified from rice root cDNA using the following primers: OsDRP1 GW F-AAAAAGCAGGCTATATGGAGAACCTGATCTCGC and Os DRP1A-HA R-TGGTACGTCGTATGGGTATTTGGACCATGC AAC. The PCR product was cloned into the pTA2 vector (Toyobo). The K47A mutation in OsDRP1A was introduced by PCR-based site-directed mutagenesis using the following two primers: OsDRP1 K47A F- GAGTTCGGGTGCATCCT CGGTGCTG and OsDRP1 K47A R- CAGCACCGAGGATGCA CCCGAACTC. HA-tag was fused at the C-terminal of OsDRP1A CDS by additional PCR using the following primers: OsDRP1 GW F and HA-GW R-AGAAAGCTGGG TTCTAAGCGTAATCTGGTACGTCG. This PCR product, OsDRP1A^{K47A}-HA, was cloned into a Gateway pDONR/Zeo Vector (Invitrogen TM, Thermo Fisher Scientific, Waltham, MA, USA). A plasmid vector harboring *Est≫OsDRP1A^{K47A}-HA*, *OsDRP1A^{K47A}-HA* was subcloned into pER8 (Zuo et al., 2000) via a Gateway LR-recombinant reaction (a recombination reaction between attL and attR sites, Invitrogen TM, Thermo Fisher Scientific). This plasmid vector was transformed into callus of Nipponbare as described above.

Knockout line of *OsAP2M* (*Os02g0690700*) gene was generated by CRISPR/Cas9 technique. The Cas9 plant expression vector (pU6gRNA) and single-guide RNA expression vector (pZDgRNA_Cas9ver.2_HPT) were kindly provided by Dr

Masaki Endo (National Institute of Agrobiological Sciences, Japan; Endo et al., 2015). Specific target sequence, GAAATATGGTTGATGCATTC located at second exon, was used for mutant generation. Synthetic guide RNA expression construct, including the target sequence, was cloned into pZDgRNACas9ver.2_HPT according to Che et al. (2019). The derived construct was transformed into calluses (cv. Nipponbare) by *A. tumefaciens*-mediated transformation as described above. To genotype the resultant mutants, genomic DNA was extracted from leaves of transgenic rice plants at T0 generation. The genomic sequence, including the target region, was amplified and directly sequenced by following primers; OsAP2M genome F; CCACTAAACATT TTCGGTTTGC, and OsAP2M genome R; TGCATACCTCCA CGACAAAC. One cytosine inserted frame-shift mutant was selected. A knockout line without T-DNA insertion was selected at T1 generation.

Homo mutated plants (−/−) and nonmutated plants (+/+) as a control were selected from the heterozygous seedlings. Seedlings (28-d-old) pretreated without B for 3 d were exposed to 0 or 30 μM B for 6 h. The roots were sampled for immunostaining of OsBOR1 as described below.

Expression response of *OsLsi1* and *OsBOR1* to different B concentrations in roots

To investigate the effect of different B concentrations on the expression of *OsLsi1* and *OsBOR1* in the roots, seedlings (21-d-old, cv. Nipponbare) were exposed to a solution containing 0, 0.3, 3 (concentration in Kimura B solution), or 30 μM B. After 7 d, the roots were sampled for RNA extraction. For a time-course experiment, seedlings (25-d-old) were precultured in B-free solution for 3 d, followed by exposing to a solution containing 30 μM B. At time points indicated (0.5, 2, and 6 h after exposure to B), the roots were sampled. Spatial expression pattern of *OsBOR1* in the roots was investigated by sampling different root segments (0–0.5, 0.5–1.0, and 1.0–2.0 cm from the root tip) from 5-d-old plants.

The total RNA was extracted by using an RNeasy Plant Mini Kit (Qiagen, Hilden, Germany), followed by DNase I treatment. Conversion to cDNA was performed using the protocol supplied by the manufacturer of Super Script II (Invitrogen, Waltham, MA, USA) and *OsLsi1* and *OsBOR1* expression analyses were performed by quantitative real-time PCR. *OsNIP3;1* was used as a B-responsive marker gene (Shao et al., 2018). *Histone H3* was used as an internal standard. The primers used were as described in Shao et al. (2018, 2021).

Immunostaining of OsBOR1 and Flag-OsLsi1

For double immunostaining of OsBOR1 and Flag-OsLsi1, selected seedlings (T1, 25-d-old) of the transgenic line carrying *Flag-OsLsi1* were precultured in a solution without B for 3 d. The localization of OsBOR1 and OsLsi1 was observed in root tip, crown root and lateral roots. For dose-dependent analysis, the seedlings (25-d-old) were precultured in B-free solution for 3 d, followed by exposing to a solution containing 0, 0.3, 3, and 30 μM B for 6 h. For a time-dependent analysis, seedlings (25-d-old) were precultured in B-free solution for 3 d, followed by exposing to a solution containing 30 μM B for 0, 0.5, 2, 6, 12, and 24 h. The cross-sections (3 or 15 mm from the root tip) were prepared and used for double immunostaining with antibodies of OsBOR1 and Flag according to Konishi and Ma (2021). Briefly, a rabbit polyclonal anti-OsBOR1 antibody (1/2,000; Shao et al., 2021) and a rat monoclonal DYKDDDDK (Flag) epitope tag antibody (1/1,000; L5, Novus Biologicals, Littleton, CO, USA) were used for immunostaining as a primary antibody. Fluorescence from the secondary antibodies (Alexa Fluor 555 goat anti-rabbit IgG for OsBOR1, Alexa Fluor 488 goat anti-rat IgG for OsLsi1; Thermo Fisher Scientific) were observed with a confocal laser scanning microscope (TCS SP8x; Leica microsystems, Wetzlar, Germany) with excitation at 555 nm (white-light laser) and emission in the range 563–580 nm for Alexa Fluor 555, and with excitation at 488 nm (white-light laser) and emission in the range 510–560 nm for Alexa Fluor 488. The *bor1-1* mutant was used as a negative control. All pictures were taken under the same conditions. The signal intensity was quantified by LAS AF Lite software version 4.0 (Leica microsystems) using 6–16 independent images. In some experiments, the signal from *bor1-1* mutant, as a background signal, was subtracted and the signal intensity relative to −B treatment was calculated.

For double immunostaining with OsBOR1 and HA, selected seedlings of the transgenic line (T1, 21-dy-old) harboring *Est≫OsDRP1A^{K47A}-HA* were precultured in a solution without B for 1 d and then subjected to a solution containing 20 μM β-estradiol (dissolved in DMSO) or the same amount of DMSO for 2 d to induce the expression of *OsDRP1A^{K47A}-HA*. To observe the degradation of OsBOR1, a final concentration of 30 μM B was added to the solution containing 20 μM β-estradiol or DMSO. After 6 h, the crown roots were sampled and the cross-sections (3 or 10 mm from the root tip) were used for double immunostaining of OsBOR1 and HA according to the method described above. Rat monoclonal Anti-HA High-Affinity antibody (1/500: 3F10, F. Hoffmann-La Roche, Ltd., Basel, Switzerland) and Alexa Fluor 488 goat anti-rat IgG were used for OsDRP1A^{K47A}-HA immunostaining as a primary and secondary antibody, respectively. After incubation with a secondary antibody, the nuclei were stained by 4′,6-diamidino-2-phenylindole (DAPI). All pictures were taken under the same conditions and the signal intensity was quantified as described above. Roots with strong and weak expression of *OsDRP1A^{K47A}-HA* were selected for observation of whole roots and cells, respectively.

Western blot analysis

Similar root samples as described above (dose- and time-dependent expression experiments) were subjected to western blot analysis with three biological replicates. Each replicate contains four plants, and the experiments were performed for three times. Extraction of total protein and

preparation of microsome fraction were performed as described previously (Mitani et al., 2009). The same amounts (10 μg) of microsome protein were subjected to SDS–PAGE using 5%–20% gradient polyacrylamide gels (e-PAGEL, ATTO, http://www.atto.co.jp) and subsequently to immunoblotting. The membrane was treated with OsBOR1 antibody (1:500 dilutions). Anti-Rabbit IgG (H + L) HRP conjugate (1:50,000 dilutions; Promega, Madison, WI, USA; http://www.promega.com) was used as a secondary antibody. ECL prime (GE Healthcare, Chicago, IL, USA) was used for detection, and the signal was captured by a ChemiDoc imager (Bio-Rad, Hercules, CA, USA). Rabbit polyclonal H^+-ATPase antibody (AS07 260, 1/3,000, Agrisera, Vännäs, Sweden) was used as a control. The band intensity relative to sample free of B was quantified by I_{MAGE} L_{AB} Software (Bio-Rad).

Response of OsBOR1 protein to B-deficiency

To investigate the response of OsBOR1 protein to B-deficiency, seedlings (21-d-old) were exposed to a solution containing 30 μM B for 3 d, followed by transferring to a solution free of B. At 0, 1, 3, and 5 d after −B treatment, the roots were sampled for immunostaining of OsBOR1 as described above. Multiple images were taken under the same condition and their fluorescence intensity was quantified as described above.

Effect of inhibitors on OsBOR1 degradation

To investigate the effect of BFA, MG-132, ConcA, and CHX on OsBOR1 degradation, transgenic seedlings (25-d-old) harboring Flag-OsLsi1 as described in above experiments were used. After pretreatment with −B for 3 d, the roots were pretreated with 50 μM BFA, 100 μM MG-132, 1 μM ConcA, or 200 μM CHX for 1 h, followed by exposure to 0 or 30 μM B in the presence and absence of the inhibitors under dark condition. All inhibitors except CHX were dissolved in DMSO. After 2 (BFA) or 6 h, the roots were sampled for immunostaining with OsBOR1 antibody or western blot analysis as described above.

FM4–64 internalization assay

Seedlings (21-d-old) of transgenic lines harboring *Est≫OsDRP1A^{K47A}-HA* were precultured in half-strength Kimura B solutions containing DMSO or 20 μM β-estradiol (dissolved in DMSO) for 2 d. The crown roots (1.5 cm from root tip) were excised and incubated in the half-strength Kimura B solutions containing 20 μM FM4–64 for 30 min in the dark at 25°C, followed by moving into a fixation solution (4% (v/v) formaldehyde, 60-mM sucrose, 50-mM cacodylic acid (pH 7.4)). After centrifuging twice (7,000 rpm for 2 min), roots were incubated for 2 h in the dark for fixation. The roots were subsequently embedded in 5% agar, and several cross-slices (2 mm from the root tip) were prepared by microslicer (LinierSlicer PRO10; Dosaka EM, Co., Ltd., Kyoto, Japan). Half of the cross-sections were used for FM4–64 observation immediately after slice preparation because the signal decline of FM4–64 was rapid. Another half of the slice was used for anti-HA immunostaining according to the method described above to determine the induction of OsDRP1A^{K47A}-HA. FM4–64 signals were observed with a confocal laser scanning microscope (TCS SP8x, Leica microsystems) with excitation at 515 nm (white light laser) and emission in the range 632–649.

Labeling experiment with the stable isotope $^{10}B/^{11}B$

A short-term (10 h) labeling experiment with $^{10}B/^{11}B$ was performed with seedlings (20-d-old) of mutants and WT. The seedlings were precultured in solution containing 30 μM ^{11}B (99% enriched H_3BO_3; Cambridge Isotope Laboratories, Tewksbury, MA, USA), followed by exposing to a solution containing 0 or 30 μM ^{11}B. After 3 d, the seedlings were subjected to a solution containing 0.3 or 30 μM ^{10}B (99% enriched H_3BO_3, Cambridge Isotope Laboratories). After 10-h labeling, the roots were washed with 5-mM $CaCl_2$ solution for 3 times and separated from the shoots. Their fresh weight was recorded and the concentration of ^{10}B was determined as described below. The root-to-shoot translocation rate of ^{10}B was calculated based on (^{10}B content in shoots/total ^{10}B content × 100%).

Determination of B concentration

Sample digestion and B determination were performed according to a previous study (Shao et al., 2018). Briefly, after dried at 70°C for at least 3 d, the samples were digested with HNO_3 (60%) and H_2O_2 (30%) mixture (HNO_3:H_2O_2 = 1:1) at a temperature up to 110°C in a 15 mL plastic tubes. After dilution, the concentration of B was determined by inductively coupled plasma mass spectrometry using an isotope mode (7700X; Agilent Technologies, Santa Clara, CA, USA).

Statistical analysis of data

Data were analyzed using Student's *t* test, and Tukey–Kramer's test at $P < 0.05$ or $P < 0.01$.

Accession numbers

Sequence data from this article can be found in the GenBank/EMBL data libraries under accession numbers, AB222272 for OsLsi1 and AK100510 for OsBOR1.

Supplemental data

The following materials are available in the online version of this article.

Supplemental Figure S1. Complementation test for Si uptake in transgenic line carrying *Flag-OsLsi1*.

Supplemental Figure S2. Spatial expression of *OsBOR1* in the roots.

Supplemental Figure S3. Time-dependent western blot analysis of OsBOR1 in response to high B concentrations in rice roots.

Supplemental Figure S4. Effect of CHX on high B-induced degradation of OsBOR1 in rice roots.

Supplemental Figure S5. Effect of *OsAP2M* knockout on the degradation and polarity of OsBOR1 in rice roots.

Supplemental Figure S6. Effect of mutated OsDRP1A^{K47A}–HA on endocytosis in rice roots.

Supplemental Figure S7. OsBOR1 signal intensity in root cells with different induction of OsDRP1A^{K47A}.

Supplemental Figure S8. Effect of BFA treatment on localization of OsBOR1 in rice roots.

Supplemental Figure S9. Effects of ConcA on localization of OsBOR1 in rice roots.

Supplemental Figure S10. Effects of MG-132 treatment on the B-induced degradation of OsBOR1 protein in rice roots.

Supplemental Figure S11. Effect of pretreatment with different B supply on the growth of WT and mutants.

Acknowledgments

We thank Akemi Morita, Yoshimi Takahashi, and Sanae Rikiishi for experimental assistance. We also thank Rice Resource Center in Tsukuba for providing *Tos-17* insertion lines and Misaki Endo for providing CRISPR/Cas9 vector.

Funding

This work was supported by Grant-in-Aid for Specially Promoted Research (JSPS KAKENHI Grant Numbers 16H06296 and 21H05034 to J.F.M.).

Conflict of interest statement. All authors state no conflict of interest concerning this paper.

References

Adams J, Stein R (1996) Novel inhibitors of the proteasome and their therapeutic use in inflammation. Annu Rep Med Chem **31**: 279–288

Aibara I, Hirai T, Kasai K, Takano J, Onouchi H, Naito S, Fujiwara T, Miwa K (2018) Boron-dependent translational suppression of the borate exporter BOR1 contributes to the avoidance of boron toxicity. Plant Physiol **177**: 759–774

Atique-ur-Rehman, Farooq M, Rashid A, Nadeem F, Stuerz S, Asch F, Bell RW, Siddique KHM (2018) Boron nutrition of rice in different production systems. A review. Agrono Sustain Dev **38**: 25

Barberon M, Zelazny E, Robert S, Conéjéro G, Curie C, Friml J, Vert G (2011) Monoubiquitin-dependent endocytosis of the iron-regulated transporter 1 (IRT1) transporter controls iron uptake in plants. Proc Natl Acad Sci USA **108**: E450–E458

Blevins DG, Lukaszewski KM (1998) Boron in plant structure and function. Annu Rev Plant Biol **49**: 481–500

Chatterjee M, Tabi Z, Galli M, Malcomber S, Buck A, Muszynski M, Gallavotti A (2014) The boron efflux transporter ROTTEN EAR is required for maize inflorescence development and fertility. Plant Cell **26**: 2962–2977

Che J, Yamaji N, Ma JF (2018) Efficient and flexible uptake system for mineral elements in plants. New Phytol **219**: 513–517

Che J, Yokosho K, Yamaji N, Ma JF (2019) A vacuolar phytosiderophore transporter alters iron and zinc accumulation in polished rice grains. Plant Physiol **181**: 276–288

Chiba Y, Mitani N, Yamaji N, Ma JF (2009) HvLsi1 is a silicon influx transporter in barley. Plant J **5**: 810–818

Coudert Y, Périn C, Courtois B, Khong NG, Gantet P (2010) Genetic control of root development in rice, the model cereal. Trends Plant Sci **15**: 219–226

Dell B, Huang L (1997) Physiological response of plants to low boron. Plant Soil **193**: 103–120

Durbak AR, Phillips KA, Pike S, O'Neill MA, Mares J, Gallavotti A, Malcomber, ST, Gassmann W, McSteen P (2014) Transport of boron by the tassel-less1 aquaporin is critical for vegetative and reproductive development in maize. Plant Cell **26**: 2978–2995

Enstone DE, Peterson CA, Ma F (2002) Root endodermis and exodermis: structure, function, and responses to the environment. J Plant Growth Regul **21**: 335–351

Eaton FM (1944) Deficiency, toxicity and accumulation of boron in plants. J Agric Res **69**: 237–279

Endo M, Mikami M, Toki S (2015) Multigene knockout utilizing off-target mutations of the CRISPR/Cas9 system in rice. Plant Cell Physiol **56**: 41–47

Finley D (2009) Recognition and processing of ubiquitin–protein conjugates by the proteasome. Annu Rev Biochem **78**: 477–513.

Geldner N, Friml J, Stierhof YD, Jürgens G, Palme K (2001) Auxin transport inhibitors block PIN1 cycling and vesicle trafficking. Nature **413**: 425–428

Hiei Y, Ohta S, Komari T, Kumashiro T (1994) Efficient transformation of rice (*Oryza sativa* L.) mediated by *Agrobacterium* and sequence analysis of the boundaries of the T-DNA. Plant J **6**: 271–282

Huang S, Wang P, Yamaji N, Ma JF (2020) Plant nutrition for human nutrition: hints from rice research and future perspectives. Mol Plant **13**: 825–835

Kasai K, Takano J, Miwa K, Toyoda A, Fujiwara T (2011) High boron-induced ubiquitination regulates vacuolar sorting of the BOR1 borate transporter in *Arabidopsis thaliana*. J Biol Chem **286**: 6175–6183

Konishi N, Ma JF (2021) Three polarly localized ammonium transporter 1 members are cooperatively responsible for ammonium uptake in rice under low ammonium condition. New Phytol **232**: 1778–1792

Leonard A, Holloway B, Guo M, Rupe M, Yu G, Beatty M, Hayes GZ, Meeley R, Llaca V, Butler K, et al. (2014) Tassel-less1 encodes a boron channel protein required for inflorescence development in maize. PlantCell Physiol **55**: 1044–1054

Li J, Yuan J, Wang H, Zhang H, Zhang H (2020) Arabidopsis COPPER TRANSPORTER 1 undergoes degradation in a proteasome-dependent manner. J Exp Bot **71**: 6174–6186

Loomis WD, Durst RW (1992) Chemistry and biology of boron. BioFactors **3**: 229–239

Ma JF, Goto S, Tamai K, Ichii M (2001) Role of root hairs and lateral roots in silicon uptake by rice. Plant Physiol **127**: 1773–1780

Ma JF, Tamai K, Ichii M, Wu GF (2002) A rice mutant defective in Si uptake. Plant Physiol **130**: 2111–2117

Ma JF, Tamai K, Yamaji N, Mitani N, Konishi S, Katsuhara M, Ishiguro M, Murata Y, Yano M (2006) A silicon transporter in rice. Nature **440**: 688–691

Ma JF, Yamaji N, Mitani N, Tamai K, Konishi S, Fujiwara T, Katsuhara M, Yano M (2007) An efflux transporter of silicon in rice. Nature **448**: 209–212

Matoh, T (1997) Boron in plant cell walls. Plant Soil **193**: 59–70

Marschner P (2012) Mineral Nutrition of Higher Plants, 3rd edn, Academic Press, London

Matthes MS, Robil JM, McSteen P (2020) From element to development: the power of the essential micronutrient boron to shape morphological processes in plants. J Exp Bot **71**: 1681–1693

Mengel K, Kirkby EA (1987) Principles of Plant Nutrition, International Potash Institute, Worblaufen-Bern, Switzerland

Mitani N, Yamaji N, Ma JF (2009) Identification of maize silicon influx transporters. Plant Cell Physiol **50**: 5–12

Mitani N, Yamaji N, Ma JF (2008) Characterization of substrate specificity of a rice silicon transporter, Lsi1. Pflugers Arch **456**: 679–686

Mitani-Ueno N, Yamaji N, Ma JF (2018) Transport system of mineral elements in rice. *In* T Sasaki, M Ashikari, eds, Rice Genomics, Genetics and Breeding, Springer Singapore, Singapore, pp 223–240

Mitani-Ueno N, Yamaji N, Zhao FJ, Ma JF (2011) The aromatic/arginine selectivity filter of NIP aquaporins plays a critical role in substrate selectivity for silicon, boron, and arsenic. J Exp Bot **62**: 4391–4398

Nable RO, Banuelos GS, Paull JG (1997) Boron toxicity. Plant Soil **193**:181–198

Nakagawa Y, Hanaoka H, Kobayashi M, Miyoshi K, Miwa K, Fujiwara T (2007) Cell-type specificity of the expression of *OsBOR1*, a rice efflux boron transporter gene, is regulated in response to boron availability for efficient boron uptake and xylem loading. Plant Cell **19**: 2624–2635

O'Neill MA, Eberhard S, Albersheim P, Darvill AG (2001) Requirement of borate crosslinking of cell wall rhamnogalacturonan II for *Arabidopsis* growth. Science **294**: 846–849

Onuh AF, Miwa K (2021) Regulation, diversity and evolution of boron transporters in plants. Plant Cell Physiol **62**: 590–599

Ooi CE, Rabinovich E, Dancis A, Bonifacino JS, Klausner RD (1996) Copper-dependent degradation of the *Saccharomyces cerevisiae* plasma membrane copper transporter Ctr1p in the apparent absence of endocytosis. EMBO J **15**: 3515–3523

Pallotta M, Schnurbusch T, Hayes J, Hay A, Baumann U, Paull J, Langridge P, Sutton T (2014) Molecular basis of adaptation to high soil boron in wheat landraces and elite cultivars. Nature **514**: 88–91

Park BS, Seo JS, Chua NH (2014) Nitrogen limitation adaptation recruits PHOSPHATE2 to target the phosphate transporter PT2 for degradation during the regulation of *Arabidopsis* phosphate homeostasis. Plant Cell **26**: 454–464

Rebouillat J, Dievart A, Verdeil JL, Escoute J, Giese G, Breitler JC, Gantet P, Espeout S, Guiderdoni E, Périn C (2009) Molecular genetics of rice root development. Rice **2**: 15–34

Robatzek S, Chinchilla D, Boller T (2006) Ligand-induced endocytosis of the pattern recognition receptor FLS2 in *Arabidopsis*. Genes Dev **20**: 537–542

Sakurai G, Satake A, Yamaji N, Mitani-Ueno N, Yokozawa M, Feugier FG, Ma JF (2015) In silico simulation modeling reveals the importance of the Caspian strip for efficient silicon uptake in rice roots. Plant Cell Physiol **56**: 631–639

Sasaki A, Yamaji N, Ma JF (2016) Transporters involved in mineral nutrient uptake in rice. J Exp Bot **67**: 3645–3653

Sasaki A, Yamaji N, Yokosho K, Ma JF (2012) Nramp5 is a major transporter responsible for manganese and cadmium uptake in rice. Plant Cell **24**: 2155–2167

Schnurbusch T, Hayes J, Hrmova M, Baumann U, Ramesh SA, Tyerman S D, Langridge P, Sutton T (2010) Boron toxicity tolerance in barley through reduced expression of the multifunctional aquaporin *HvNIP2;1*. Plant Physiol **153**: 1706–1715

Shao JF, Yamaji N, Liu XW, Yokosho K, Shen RF, Ma JF (2018) Preferential distribution of boron to developing tissues is mediated by the intrinsic protein OsNIP3. Plant Physiol **176**: 1739–1750

Shao JF, Yamaji N, Huang S, Ma JF (2021) Fine regulation system for distribution of boron to different tissues in rice. New Phytol **230**: 656–668

Shin LJ, Lo JC, Chen GH, Callis J, Fu H, Yeh KC (2013) IRT1 degradation factor1, a ring E3 ubiquitin ligase, regulates the degradation of iron-regulated transporter1 in *Arabidopsis*. Plant Cell **25**: 3039–3051

Shorrocks VM (1997) The occurrence and correction of boron deficiency. Plant Soil **193**: 121–148

Sutton T, Baumann U, Hayes J, Collins NC, Shi BJ, Schnurbusch T, Hay A, Mayo G, Pallotta M, Tester M, et al. (2007) Boron-toxicity tolerance in barley arising from efflux transporter amplification. Science **318**: 1446–1449

Takano J, Miwa K, Yuan L, von Wirén N, Fujiwara T (2005) Endocytosis and degradation of BOR1, a boron transporter of *Arabidopsis thaliana*, regulated by boron availability. Proc Natl Acad Sci USA **102**: 12276–12281.

Takano J, Noguchi K, Yasumori M, Kobayashi M, Gajdos Z, Miwa K, Hayashi, H, Yoneyama T, Fujiwara T (2002) Arabidopsis boron transporter for xylem loading. Nature **420**: 337–340

Takano J, Tanaka M, Toyoda A, Miwa K, Kasai K, Fuji K, Onouchi H, Naito S, Fujiwara T (2010) Polar localization and degradation of *Arabidopsis* boron transporters through distinct trafficking pathways. Proc Natl Acad Sci USA **107**: 5220–5225

Takano J, Wada M, Ludewig U, Schaaf G, Von Wirén N, Fujiwara T (2006) The *Arabidopsis* major intrinsic protein NIP5;1 is essential for efficient boron uptake and plant development under boron limitation. Plant Cell **18**: 1498–1509

Tanaka M, Takano J, Chiba Y, Lombardo F, Ogasawara Y, Onouchi H, Naito S, Fujiwara T (2011) Boron-dependent degradation of *NIP5;1* mRNA for acclimation to excess boron conditions in Arabidopsis. Plant Cell **23**: 3547–3559

Tanaka M, Sotta N, Yamazumi Y, Yamashita Y, Miwa K, Murota K, Chiba Y, Hirai MY, Akiyama T, Onouchi H, et al. (2016) The minimum open reading frame, AUG-stop, induces boron-dependent ribosome stalling and mRNA degradation. Plant Cell **28**: 2830–2849

Ueno D, Sasaki A, Yamaji N, Miyaji T, Fujii Y, Takemoto Y, Moriyama S, Che J, Moriyama Y, Iwasaki K, et al. (2015) A polarly localized transporter for efficient manganese uptake in rice. Nat Plants **1**: 1–8

Wang L, Li H, Lv X, Chen T, Li R, Xue Y, Jiang J, Jin B, Baluška F, Šamaj J, et al. (2015) Spatiotemporal dynamics of the BRI1 receptor and its regulation by membrane microdomains in living *Arabidopsis* cells. Mol Plant **8**: 1334–1349

Wang S, Yoshinari A, Shimada T, Hara-Nishimura I, Mitani-Ueno N, Ma JF, Naito S, Takano J (2017) Polar localization of the NIP5; 1 boric acid channel is maintained by endocytosis and facilitates boron transport in Arabidopsis roots. Plant Cell **29**: 824–842

Wu XW, Lu XP, Riaz M, Yan L, Jiang CC (2019) Boron toxicity induced different changes of the cell ultrastructure and architecture of components in different leaf segments of trifoliate orange. J Environ Manage **246**: 426–433

Yamaji N, Ma JF (2007) Spatial distribution and temporal variation of the rice silicon transporter Lsi1. Plant Physiol **143**:1306–1313

Yamaji N, Ma JF (2021) Metalloid trasporters and their regulation in plants. Plant Physiol **187**: 1929–1939

Yoshinari A, Fujimoto M, Ueda T, Inada N, Naito S, Takano J (2016) DRP1-dependent endocytosis is essential for polar localization and boron induced degradation of the borate transporter BOR1 in *Arabidopsis thaliana*. Plant Cell Physiol **57**: 1985–2000

Yoshinari A, Hosokawa T, Amano T, Beier MP, Kunieda T, Shimada T, Hara-Nishimura I, Naito S, Takano J (2019) Polar localization of the borate exporter BOR1 requires AP2-dependent endocytosis. Plant Physiol **179**: 1569–1580

Yoshinari A, Hosokawa T, Beier MP, Oshima K, Ogino Y, Hori C, Takasuka TE, Fukao Y, Fujiwara T, Takano J (2021) Transport-coupled ubiquitination of the borate transporter BOR1 for its boron-dependent degradation. Plant Cell **33**: 420–438

Yoshinari A, Takano J (2017) Insights into the mechanisms underlying boron homeostasis in plants. Front Plant Sci **8**: 1951

Zhang Q, Chen H, He M, Zhao Z, Cai H, Ding G, Shi L, Xu F (2017) The boron transporter *BnaC4.BOR1;1c* is critical for inflorescence development and fertility under boron limitation in *Brassica napus*. Plant Cell Environ **40**: 1819–1833

Zhang Y, Persson S, Hirst J, Robinson MS, Van Damme D, Sánchez-Rodríguez C (2015) Change your TPLATE, change your fate: plant CME and beyond. Trends Plant Sci **20**: 41–48

Zuo JR, Niu QW, Chua NH (2000) An estrogen receptor-based transactivator XVE mediates highly inducible gene expression in transgenic plants. Plant J **24**: 265–273